Journal of Sound and Vibration 329 (2010) 5474–5488

Contents lists available at ScienceDirect

Journal of Sound and Vibration

journal homepage: www.elsevier.com/locate/jsvi

On the forced response of waveguides using the wave and finite element method

Jamil M. Renno*, Brian R. Mace

Institute of Sound and Vibration Research, University of Southampton, Highfield, Southampton SO17 1BJ, United Kingdom

ARTICLE INFO

Article history:
Received 6 November 2009
Received in revised form
5 July 2010
Accepted 12 July 2010
Handling Editor: D. Juve
Available online 10 August 2010

ABSTRACT

The forced response of waveguides subjected to time harmonic loading is treated. The approach starts with the wave and finite element (WFE) method where a segment of the waveguide is modeled using traditional finite element methods. The mass and stiffness matrices of the segment are used to formulate an eigenvalue problem whose solution yields the wave properties of the waveguide. The WFE formulation is used to obtain the response of the waveguide to a convected harmonic pressure (CHP). Since the Fourier transform of the response to a general excitation is a linear combination of the responses to CHPs, the response to a general excitation can be obtained via an inverse Fourier transform process. This is evaluated analytically using contour integration and the residue theorem. Hence, the approach presented herein enables the response of a waveguide to general loading to be found by: (a) modeling a segment of the waveguide using finite element methods and post-processing it to obtain the wave characteristics, (b) using Fourier transform and contour integration to obtain the wave amplitudes and (c) using the wave amplitudes to find the response at any point in the waveguide. Numerical examples are presented.

1. Introduction

The dynamic response of simple structures (rods, beams, etc.) can be obtained analytically. However, for complicated structures, this can be a formidable task, if at all possible. Often, finite element analysis (FEA) is used, but finite element (FE) models can become impractically large at high frequencies, bringing an assortment of problems (memory capacity issues, accuracy, computation cost and time, etc.). An alternative is wave-based methods, which yield information about wave propagation characteristics (wavenumber, wavemodes, group velocity, modal density, etc.). This is of great value for many applications such as disturbance propagation, energy transmission, structure-borne sound, statistical energy analysis and so on.

Many structures can be regarded as waveguides, i.e. the structure is uniform in one direction. The cross-section of the waveguide can be arbitrarily complex, but must have the same geometric and physical properties at every point along the axis of the waveguide, x, as shown in Fig. 1.

Analytical solutions are available for wave propagation in simple waveguides (rods, beams, etc.), [1], while approximate solutions are often sought for complex waveguides. It is here that FEA can be used. Within this category, one approach is the "spectral finite element" (SFE) method where the displacement field is assumed separable and the response for free wave propagation is of the form e^{-ikx} along the waveguide axis. An eigenvalue problem is then formulated and solved.

* Corresponding author.
E-mail addresses: renno@isvr.soton.ac.uk (J.M. Renno), brm@isvr.soton.ac.uk (B.R. Mace).

0022-460X/$ - see front matter © 2010 Elsevier Ltd. All rights reserved.
doi:10.1016/j.jsv.2010.07.009

Nomenclature

A	cross-sectional area, m^2
E	Young's modulus of elasticity, N/m^2
G	shear modulus, N/m^2
$\mathbf{I}$	identity matrix of appropriate dimensions
I	area moment of inertia, m^4
L	length, m
U	axial displacement, m
W	transverse displacement, m
Y	mobility, m/N s
b	width, m
h	thickness, m
k	wavenumber of the structure, m^{-1}
t	time, s
x, y, z	coordinates along the corresponding axes, m
ω	excitation frequency, rad/s
ρ	mass density, kg/m^3
ν	Poisson's ratio, dimensionless
γ	wavenumber of the excitation, m^{-1}

Superscripts

T	matrix transpose
+	quantity pertaining to a positive-going wave
−	quantity pertaining to a negative-going wave.

Subscripts

L	quantity pertaining to the left end of the segment
R	quantity pertaining to the right end of the segment
x, y, z	quantity/property pertaining in the respective direction
r	quantity related to the response
e	quantity related to the excitation

The major difficulty of the SFE method is that new spectral mass and stiffness matrices are required on a case-by-case basis, which can be a significant task in itself, e.g. Refs. [2–4].

An alternative approach is to model a small segment of the waveguide using conventional FE methods, and then apply periodicity conditions. This approach is termed the wave and finite element (WFE) method, and its formulation leads to an eigenvalue problem whose solution yields the wave characteristics. The advantages of this approach are two-fold. First, the full power of existing FE methods can be harnessed. Commercial FEA packages and existing element libraries can be used to model a segment and hence there is no need for new types of elements or FEA formulations. Second, even for waveguides of complex cross-sections, the size of the model will generally be very small, circumventing the problems FEA encounters at high frequencies.

The WFE method has been used to study the free [5] and forced [6] vibration of waveguides. Earlier formulations can be found in Refs. [7,8] where the focus was on the vibration of rail tracks using periodic structure theory. The WFE method for waveguides has also been used to study thin-walled structures [9], laminated plates [5] and fluid-filled pipes [10,11]. The WFE method has also been extended to two-dimensional plane [12] and cylindrical structures [13].

In this paper, a new approach for obtaining the forced response of waveguides to arbitrary excitations based on the WFE method is presented. First, a segment of the waveguide is modeled using standard FE methods, and then the WFE approach is used to find the wave properties of the waveguide. The response of the structure when excited with a convected harmonic pressure (CHP) is then obtained. For a general excitation (whose spatial dependence is separable in the manner described in Section 3), the Fourier transform can be used to write the general excitation as a superposition of CHPs. Then, the Fourier transform of the response to the general excitation is presented as a superposition of the responses to CHPs. Thus, the response to the general excitation can be obtained via an inverse Fourier transform and this is evaluated analytically by contour integration and the residue theorem. Previous work considered the response to a point force [6,14,15]. However, the formulation presented in this manuscript allows the response to more general, time harmonic excitation to be found by using the Fourier transform and contour integration techniques.

This paper is organized as follows: in Section 2, the WFE method is summarized. Then, the formulation of the response to a general excitation is presented in Section 3. The response to a CHP is first found and then the response to general excitation is expressed as an inverse Fourier transform that is evaluated analytically using contour integration and the residue theorem. Illustrative examples are included in Section 4 and conclusions to this work are drawn in Section 5.

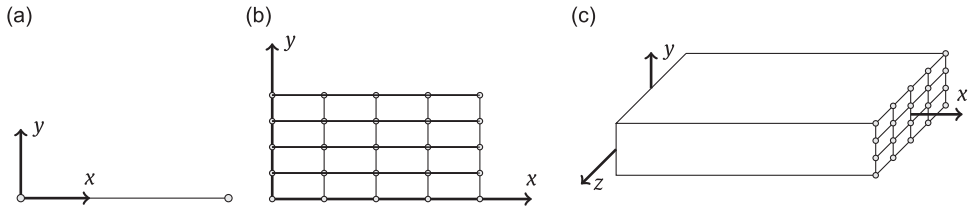

Fig. 1. Waveguides with a (a) zero-dimensional, (b) one-dimensional and (c) two-dimensional cross-section.

2. Review of the wave and finite element method

In this section a brief overview of the WFE method is presented first. Then the physical degrees of freedom (DOFs) are projected onto the wave basis and the response of waveguides to point excitation is found.

2.1. Free wave propagation and the wave basis

The WFE method starts with obtaining the model of a segment of a waveguide, Fig. 2. This can be done using any FEA package with the only constraint being that the nodes and their DOFs are ordered identically on the left and right sides of the segment. Internal nodes can be eliminated via dynamic condensation [15]. The length of the segment, Δ, should not be too large compared to the shortest wavelength; otherwise the discretized model will not accurately describe the motion of the waveguide. On the other hand, Δ should not be too small compared to the shortest wavelength to avoid machine round-off errors [15].

Time harmonic dependence of the form $e^{i\omega t}$ is assumed throughout this work and is suppressed for brevity. The governing equation of the segment of Fig. 2 is

$$[\mathbf{K}-\omega^2\mathbf{M}]\mathbf{q}=\mathbf{f}+\mathbf{e}, \tag{1}$$

where $\mathbf{q}$, $\mathbf{f}$ and $\mathbf{e}$ are $(2n\times 1)$ vectors of nodal DOFs, internal and external nodal forces, respectively, and $\mathbf{M}$ and $\mathbf{K}$ are the mass and stiffness matrices of the segment. Damping can be included by a viscous damping matrix $\mathbf{C}$ or by $\mathbf{K}$ being complex. The dynamic stiffness matrix $\mathbf{D}=\mathbf{K}-\omega^2\mathbf{M}$ can be partitioned to reflect the influence of the left and right nodes of the segment. Hence, for free wave propagation, Eq. (1) is expressed as

$$\begin{bmatrix}\mathbf{D}_{LL} & \mathbf{D}_{LR}\\ \mathbf{D}_{RL} & \mathbf{D}_{RR}\end{bmatrix}\begin{Bmatrix}\mathbf{q}_L\\ \mathbf{q}_R\end{Bmatrix}=\begin{Bmatrix}\mathbf{f}_L\\ \mathbf{f}_R\end{Bmatrix}. \tag{2}$$

When a wave propagates freely through the waveguide, the propagation constant $\lambda=e^{-ik\Delta}$ relates the right and left nodal DOFs and forces by

$$\mathbf{q}_R=\lambda\mathbf{q}_L,\quad \mathbf{f}_R=-\lambda\mathbf{f}_L. \tag{3}$$

Eq. (2) is rearranged into

$$\lambda\begin{Bmatrix}\mathbf{q}_L\\ \mathbf{f}_L\end{Bmatrix}=\mathbf{T}\begin{Bmatrix}\mathbf{q}_L\\ \mathbf{f}_L\end{Bmatrix}, \tag{4}$$

where

$$\mathbf{T}=\begin{bmatrix}-\mathbf{D}_{LR}^{-1}\mathbf{D}_{LL} & \mathbf{D}_{LR}^{-1}\\ -\mathbf{D}_{RL}+\mathbf{D}_{RR}\mathbf{D}_{LR}^{-1}\mathbf{D}_{LL} & -\mathbf{D}_{RR}\mathbf{D}_{LR}^{-1}\end{bmatrix} \tag{5}$$

is the transfer matrix. The eigenvalue problem of Eq. (4) is solved to yield the propagation constants λ_j and the corresponding wavenumbers k_j ($j=1,\ldots,2n$). For complicated waveguides with many DOFs at each node, care needs to be taken when solving this eigenvalue problem as various numerical problems may arise [15]. The eigenvalue problem is usually then recast into one of a number of better-conditioned forms [16].

It has been shown [16,17] that the eigenvalues of the transfer matrix occur in reciprocal pairs as λ_j^+ and $\lambda_j^-=1/\lambda_j^+$ with wavenumbers k_j^+ and $k_j^-=-k_j^+$, corresponding to positive- and negative-going waves, respectively. Associated with these eigenvalues are the positive- and negative-going eigenvectors $\boldsymbol{\phi}_j^+$ and $\boldsymbol{\phi}_j^-$, respectively, which will also be referred to as wavemodes. As per Eq. (4), every wavemode can be partitioned into a displacement and a force sub-vector

$$\boldsymbol{\phi}_j=\begin{Bmatrix}\boldsymbol{\phi}_q\\ \boldsymbol{\phi}_f\end{Bmatrix}_j. \tag{6}$$

Positive-going waves are characterized by

$$\begin{aligned}&\left|\lambda_j^+\right|\le 1,\\ &\mathrm{Re}\{\mathbf{f}_L^T\dot{\mathbf{q}}_L\}=\mathrm{Re}\{i\omega\mathbf{f}_L^T\mathbf{q}_L\}<0\quad\text{if}\quad\left|\lambda_j^+\right|=1,\end{aligned} \tag{7}$$

Fig. 2. FE segment of a waveguide.

which states that if the wave is traveling in the positive direction, then its amplitude should be decreasing or that if its amplitude remains constant, then there is time average power transmission in the positive direction.

With the positive- and negative-going waves identified, one could group the wavemodes as

$$\boldsymbol{\Phi}^{+}=\begin{bmatrix}\boldsymbol{\phi}_1^{+} & \cdots & \boldsymbol{\phi}_n^{+}\end{bmatrix},\quad \boldsymbol{\Phi}^{-}=\begin{bmatrix}\boldsymbol{\phi}_1^{-} & \cdots & \boldsymbol{\phi}_n^{-}\end{bmatrix},\quad \boldsymbol{\Phi}=\begin{bmatrix}\boldsymbol{\Phi}^{+} & \boldsymbol{\Phi}^{-}\end{bmatrix}. \tag{8}$$

It is also advantageous to obtain the left eigenvectors of the transfer matrix. These are $(1\times 2n)$ vectors which can be partitioned as

$$\boldsymbol{\psi}_j=[\boldsymbol{\psi}_f \quad \boldsymbol{\psi}_q]_j, \tag{9}$$

and further grouped into

$$\boldsymbol{\Psi}=\begin{bmatrix}\boldsymbol{\Psi}^{+}\\ \boldsymbol{\Psi}^{-}\end{bmatrix}. \tag{10}$$

The left and right wavemodes are orthogonal, and can be normalized so that

$$\boldsymbol{\Psi}^{+}\boldsymbol{\Phi}^{+}=\mathbf{I},\quad \boldsymbol{\Psi}^{-}\boldsymbol{\Phi}^{-}=\mathbf{I}. \tag{11}$$

A useful consequence of this normalization is that

$$\boldsymbol{\Psi}\mathbf{T}\boldsymbol{\Phi}=diag(\lambda_j), \tag{12}$$

where diag(·) represents a diagonal matrix.

The partitions of the left and right eigenvectors can be used to form the matrices

$$\boldsymbol{\Phi}_q^{+}=\begin{bmatrix}\boldsymbol{\phi}_{q,1}^{+} & \cdots & \boldsymbol{\phi}_{q,n}^{+}\end{bmatrix},\quad \boldsymbol{\Psi}_q^{+}=\begin{bmatrix}\boldsymbol{\psi}_{q,1}^{+}\\ \vdots\\ \boldsymbol{\psi}_{q,n}^{+}\end{bmatrix}. \tag{13}$$

Similar expressions hold for $\boldsymbol{\Phi}_q^{-},\boldsymbol{\Psi}_q^{-},\boldsymbol{\Phi}_f^{\pm}$ and $\boldsymbol{\Psi}_f^{\pm}$. These matrices, together with the orthogonality relations of Eq. (11), define transformations between the physical domain, where the motion is described in terms of $\mathbf{q}$ and $\mathbf{f}$, and the wave domain, where the motion is described in terms of waves of amplitudes $\mathbf{a}^{+}$ and $\mathbf{a}^{-}$ traveling in the positive and negative directions, respectively. Specifically

$$\mathbf{q}_L=\boldsymbol{\Phi}_q^{+}\mathbf{a}^{+}+\boldsymbol{\Phi}_q^{-}\mathbf{a}^{-};\quad \mathbf{f}_L=\boldsymbol{\Phi}_f^{+}\mathbf{a}^{+}+\boldsymbol{\Phi}_f^{-}\mathbf{a}^{-}, \tag{14}$$

or

$$\begin{Bmatrix}\mathbf{q}_L\\ \mathbf{f}_L\end{Bmatrix}=\boldsymbol{\Phi}\mathbf{a};\quad \mathbf{a}=\begin{Bmatrix}\mathbf{a}^{+}\\ \mathbf{a}^{-}\end{Bmatrix}. \tag{15}$$

In practice, as in modal analysis, only m pairs of (positive- and negative-going) waves might be retained, so that $\boldsymbol{\Phi}_{q,f}^{\pm}$ and $\boldsymbol{\Psi}_{q,f}^{\pm}$ are $n\times m$ and $m\times n$ matrices, respectively. The number retained can be different at different frequencies. All the propagating waves, for which $|\lambda|=1$, must be retained together with the least-rapidly attenuating waves, i.e. for $|\lambda|<1$, all those for which $|\lambda|>0.1$, or some other user-defined criterion. The reasons for reducing the size of the wave basis are partly that the size of the model will be smaller, but primarily that the calculation of the high-order wavemodes, which decay very rapidly with distance (by orders of magnitude over the segment length) and thus have a negligible contribution to the response, is very prone to poor numerical conditioning [15]. They can contaminate all subsequent calculations if they are not removed.

2.2. Response of an infinite waveguide to a point excitation

The response of an infinite waveguide to a concentrated load can now be examined. The following is briefly summarized from Ref. [15]. A point excitation $\mathbf{f}_e$ acting at the origin will generate positive- and negative-going waves of amplitudes $\mathbf{a}^{+}$ and $\mathbf{a}^{-}$ which will propagate away from the excitation point to the right and left, respectively, Fig. 3. Continuity and

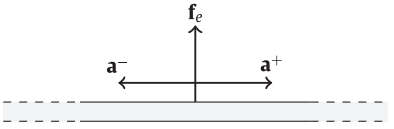

Fig. 3. Wave amplitudes generated by a point excitation.

equilibrium equations can be written at the excitation point and projected onto the wave basis to give

$$\begin{bmatrix} \mathbf{\Phi}_q^+ & -\mathbf{\Phi}_q^- \\ \mathbf{\Phi}_f^+ & -\mathbf{\Phi}_f^- \end{bmatrix} \begin{Bmatrix} \mathbf{a}^+ \\ \mathbf{a}^- \end{Bmatrix} = \begin{Bmatrix} \mathbf{0} \\ \mathbf{f}_e \end{Bmatrix}. \tag{16}$$

The orthonormalization approach presented in Eq. (11) can be used to avoid inverting the system matrix in Eq. (16) (which can lead to numerical problems [15]), and hence premultiplying by the left eigenvectors yields

$$\mathbf{a}^+ = \mathbf{\Psi}_q^+ \mathbf{f}_e, \quad \mathbf{a}^- = -\mathbf{\Psi}_q^- \mathbf{f}_e. \tag{17}$$

Next, the response to general (but separable) excitation is considered. First, the amplitudes of waves generated by a general load are obtained. Then, the response of finite waveguides is discussed.

3. Response to general excitation

The response of waveguides to general, time harmonic loading will now be formulated. The following treatment is applicable to waveguides with a zero-, one-, or two-dimensional cross-section (Fig. 1). The loading can be a vectorial quantity with components acting along any of the coordinate axes and the only restriction imposed is that every component can be written in the form $p(x, y, z, t)=p_x(x)p_{yz}(y, z)e^{i\omega t}$. In other words, the spatial part of every component can be separated into variation along the waveguide, $p_x(x)$, and over the waveguide's cross-section, $p_{yz}(y, z)$. For instance, the waveguide in Fig. 1c can be excited along the three axes. In this case, the loading will have the form

$$\mathbf{p}(x,y,z,t) = \begin{Bmatrix} p^x(x,y,z,t) \\ p^y(x,y,z,t) \\ p^z(x,y,z,t) \end{Bmatrix} = \begin{Bmatrix} p_x^x(x)p_{yz}^x(y,z) \\ p_x^y(x)p_{yz}^y(y,z) \\ p_x^z(x)p_{yz}^z(y,z) \end{Bmatrix} e^{i\omega t}, \tag{18}$$

where the superscripts x, y and z indicate the direction of the components of $\mathbf{p}$. The developments presented below are for one component. Since all the components of the loading will be later resolved into consistent nodal forces, the contributions of additional components can be simply added to the consistent nodal forces.

One approach to finding the response would be to determine the response to an excitation $\delta(x)p_{yz}(y, z)$ as described in Section 2.2 and then convolve this response with the loading $p_x(x)$. This is perhaps the simplest approach for point or very localized forces. An alternative approach that is more appealing for finding the response of waveguides to distributed loads is developed below. The cornerstone in this approach is obtaining the response to a CHP of the form $e^{-i\gamma x}p_{yz}(y, z)$, which will be treated first, and then using a Fourier decomposition of $p_x(x)$ and an inverse Fourier transform to determine the total response. This inverse transform can be evaluated analytically by contour integration, yielding the forced response at very little cost.

3.1. Response to unit amplitude convected harmonic pressure

The response to unit amplitude CHP acting along the axis of the waveguide will serve as the kernel for general loading conditions. For a zero-dimensional cross-section, a CHP takes the form $p(x)=e^{-i\gamma x}$, whereas for a one-dimensional cross-section it is $p(x, y)=e^{-i\gamma x}p_y(y)$. In a similar fashion, when the cross-section is two-dimensional, $p(x, y, z)=e^{-i\gamma x}p_{yz}(y, z)$ indicating the distribution of the excitation over the cross-section. The harmonic load over the segment is resolved to find the nodal forces applied at the ends of the segment. Moreover, the propagation constant for the forced vibration of the waveguide is now $\mu=e^{-i\gamma\Delta}$, which is imposed by the CHP. Consequently, the right and left nodal displacements and forces are related through

$$\mathbf{q}_R = \mu\mathbf{q}_L, \quad \mathbf{f}_R = -\mu\mathbf{f}_L. \tag{19}$$

The forced form of Eq. (2) is

$$\begin{bmatrix} \mathbf{D}_{LL} & \mathbf{D}_{LR} \\ \mathbf{D}_{RL} & \mathbf{D}_{RR} \end{bmatrix} \begin{Bmatrix} \mathbf{q}_L \\ \mathbf{q}_R \end{Bmatrix} = \begin{Bmatrix} \mathbf{f}_L \\ \mathbf{f}_R \end{Bmatrix} + \begin{Bmatrix} \mathbf{e}_L \\ \mathbf{e}_R \end{Bmatrix}. \tag{20}$$

The external excitation could merely be lumped at the nodes. Preferably, consistent nodal forces can be calculated as follows. If the segment is one element long then $\mathbf{e}_L$ and $\mathbf{e}_R$ can be obtained through

$$\begin{Bmatrix} \mathbf{e}_L \\ \mathbf{e}_R \end{Bmatrix} = \int_{\Sigma} e^{-i\gamma x} p_{yz}(y,z)\mathbf{N}^T(x,y,z)\, d\Sigma, \tag{21}$$

where $\mathbf{N}(x, y, z)$ is the vector of shape functions of the FE discretization process, and Σ is the integration domain (i.e. the integral is over the cross-section and the length of the element). If there are internal nodes, consistent nodal forces can be calculated for each and combined via dynamic condensation to yield $\mathbf{e}_L$ and $\mathbf{e}_R$ at the ends of the segment. Eq. (20) can be rearranged into

$$\begin{Bmatrix} \mathbf{q}_R \\ -\mathbf{f}_R \end{Bmatrix} = \mathbf{T} \begin{Bmatrix} \mathbf{q}_L \\ \mathbf{f}_L \end{Bmatrix} + \begin{bmatrix} \mathbf{D}_{LR}^{-1} & 0 \\ -\mathbf{D}_{RR}\mathbf{D}_{LR}^{-1} & \mathrm{I} \end{bmatrix} \begin{Bmatrix} \mathbf{e}_L \\ \mathbf{e}_R \end{Bmatrix}. \tag{22}$$

Now, the periodicity conditions of Eqs. (19) are invoked, to obtain

$$[\mu\mathbf{I}-\mathbf{T}]\begin{Bmatrix}\mathbf{q}_L\\ \mathbf{f}_L\end{Bmatrix}=\begin{bmatrix}\mathbf{D}_{LR}^{-1} & \mathbf{0}\\ -\mathbf{D}_{RR}\mathbf{D}_{LR}^{-1} & \mathbf{I}\end{bmatrix}\begin{Bmatrix}\mathbf{e}_L\\ \mathbf{e}_R\end{Bmatrix}. \tag{23}$$

Numerical problems might arise when inverting the system matrix $[\mu\mathbf{I}-\mathbf{T}]$ in the above equation [15]. These can be avoided by decomposing $\mathbf{q}_L$ and $\mathbf{f}_L$ into the wave domain, and exploiting the orthonormality properties of the wavemodes. Substituting Eq. (15) in Eq. (23), premultiplying by $\mathbf{\Psi}$ and using Eqs. (11) and (12) gives

$$[\mu\mathbf{I}-diag(\lambda_j)]\mathbf{a}=\mathbf{\Psi}\begin{bmatrix}\mathbf{D}_{LR}^{-1} & \mathbf{0}\\ -\mathbf{D}_{RR}\mathbf{D}_{LR}^{-1} & \mathbf{I}\end{bmatrix}\begin{Bmatrix}\mathbf{e}_L\\ \mathbf{e}_R\end{Bmatrix}. \tag{24}$$

The matrix on the left is diagonal and can be easily inverted to obtain

$$\begin{Bmatrix}\mathbf{q}_L\\ \mathbf{f}_L\end{Bmatrix}=\mathbf{\Phi}a=\mathbf{\Phi}\,diag\left(\frac{1}{\mu-\lambda_j}\right)\mathbf{\Psi}\begin{bmatrix}\mathbf{D}_{LR}^{-1} & \mathbf{0}\\ -\mathbf{D}_{RR}\mathbf{D}_{LR}^{-1} & \mathbf{I}\end{bmatrix}\begin{Bmatrix}\mathbf{e}_L\\ \mathbf{e}_R\end{Bmatrix}. \tag{25}$$

Again, although the system has n pairs of (positive- and negative-going) waves, only m pairs can be retained and used in the wave expansion. Eq. (25) can also be used to find the response at x_r, i.e.

$$\begin{Bmatrix}\mathbf{q}(x_r)\\ \mathbf{f}(x_r)\end{Bmatrix}=\mathbf{\Phi}\,diag\left(\frac{e^{-i\gamma x_r}}{\mu-\lambda_j}\right)\mathbf{\Psi}\begin{bmatrix}\mathbf{D}_{LR}^{-1} & \mathbf{0}\\ -\mathbf{D}_{RR}\mathbf{D}_{LR}^{-1} & \mathbf{I}\end{bmatrix}\begin{Bmatrix}\mathbf{e}_L\\ \mathbf{e}_R\end{Bmatrix}, \tag{26}$$

where $\mathbf{q}(x_r)$ and $\mathbf{f}(x_r)$ are $n\times 1$ vectors of the DOFs and forces at x_r. This formulation will prove useful in the next section, where the response to general excitation is considered.

3.2. General excitation

Often, waveguides are excited by spatially distributed loads where $p(x, y, z)$ could be arbitrary. In the following formulation, the only restriction imposed on $p(x, y, z)$ is that it can be written as $p(x, y, z)=p_x(x)p_{yz}(y, z)$. The treatment starts with decomposing $p(x, y, z)$ by partial Fourier transform into

$$p(x,y,z)=\frac{p_{yz}(y,z)}{\sqrt{2\pi}}\int_{-\infty}^{\infty}\overline{p}_x(\gamma)e^{-i\gamma x}\,d\gamma, \tag{27}$$

where

$$\overline{p}_x(\gamma)=\frac{1}{\sqrt{2\pi}}\int_{-\infty}^{\infty}p_x(x)e^{i\gamma x}\,dx \tag{28}$$

is the Fourier transform of $p_x(x)$. The inverse Fourier transform allows the expression of the spatial function $p(x, y, z)$ as a linear combination of CHPs, and thus, by linearity of Eq. (20), the response to $p(x, y, z)$ is a linear combination of the response to a CHP, namely

$$\begin{Bmatrix}\mathbf{q}(x_r)\\ \mathbf{f}(x_r)\end{Bmatrix}=\mathbf{\Phi}\mathbf{a}(x_r)=\frac{1}{\sqrt{2\pi}}\mathbf{\Phi}\int_{-\infty}^{\infty}diag\left(\frac{\overline{p}_x(\gamma)e^{-i\gamma x_r}}{\mu-\lambda_j}\right)\mathbf{\Psi}\begin{bmatrix}\mathbf{D}_{LR}^{-1} & \mathbf{0}\\ -\mathbf{D}_{RR}\mathbf{D}_{LR}^{-1} & \mathbf{I}\end{bmatrix}\begin{Bmatrix}\mathbf{e}_L\\ \mathbf{e}_R\end{Bmatrix}d\gamma \tag{29}$$

in Eq. (21).

The integral in Eq. (29) can be evaluated analytically by contour integration and the residue theorem. From Eq. (29), the wave amplitudes at point x_r are

$$\begin{Bmatrix}\mathbf{a}^+(x_r)\\ \mathbf{a}^-(x_r)\end{Bmatrix}=\frac{1}{\sqrt{2\pi}}\int_{-\infty}^{\infty}diag\left(\frac{e^{-i\gamma x_r}\overline{p}_x(\gamma)}{\mu-\lambda_j}\right)\mathbf{\Psi}\begin{bmatrix}\mathbf{D}_{LR}^{-1} & \mathbf{0}\\ -\mathbf{D}_{RR}\mathbf{D}_{LR}^{-1} & \mathbf{I}\end{bmatrix}\begin{Bmatrix}\mathbf{e}_L\\ \mathbf{e}_R\end{Bmatrix}d\gamma. \tag{30}$$

The wave amplitude a_j^+ of the jth positive-going wavemode can be written as

$$a_j^+(x_r)=\frac{1}{\sqrt{2\pi}}\int_{-\infty}^{\infty}\left\{\frac{e^{-i\gamma x_r}\overline{p}_x(\gamma)g_j^+(\gamma)}{\mu-\lambda_j^+}\right\}d\gamma, \tag{31}$$

where

$$g_j^+(\gamma)=\mathbf{\psi}_j^+\begin{bmatrix}\mathbf{D}_{LR}^{-1} & \mathbf{0}\\ -\mathbf{D}_{RR}\mathbf{D}_{LR}^{-1} & \mathbf{I}\end{bmatrix}\begin{Bmatrix}\mathbf{e}_L(\gamma)\\ \mathbf{e}_R(\gamma)\end{Bmatrix},\quad j=1,\ldots,m. \tag{32}$$

The contour of integration is closed in the lower or upper complex γ half-plane as shown in Fig. 4. The choice depends on the convergence of the integral around the semi-circular segments Γ_1 and Γ_2, where $\gamma = R\,e^{i\theta}$ and $R \to \infty$. From the residue theorem, the integrals around the contours $C_1 = \Gamma_1 \cup \Gamma_0$ and $C_2 = \Gamma_2 \cup \Gamma_0$ are then $\pm 2\pi i \sum \mathrm{Res}(\gamma_0)$, respectively, where the sum is of the residues of all the poles γ_0 within the contour.

The choice of contour depends on the excitation and response locations. If x_r is to the right of the loaded area ($x_r \geq x_e$, $\forall x_e$), then the contour should be closed in the lower half-plane (Fig. 4b). For example, for a point force f_e applied at point $x_e \leq x_r$, $\overline{p}_x(\gamma) = e^{i\gamma x_e} f_e/\sqrt{2\pi}$ and the numerator of the integrand involves the term $e^{-i\gamma(x_r - x_e)}$ which tends to zero on Γ_2. Similarly, if ($x_r \leq x_e$, $\forall x_e$), the contour is closed in the upper half-plane along Γ_1. (If x_r is within the excited region the integrand is split into two parts, Γ_1 and Γ_2 being chosen for the respective parts.)

Returning to Eq. (31), the poles of the integrand lie at

$$\gamma_0 = k_j^+ + \frac{2p\pi}{\Delta}, \quad j = 1,\ldots,2m; \quad p \in \mathbb{Z}. \tag{33}$$

The poles other than when $p=0$ are artifacts of the FE discretization process, and their contribution will be neglected. If their contribution is significant this implies that the FE discretization is not fine enough. Thus, only the residue of the pole located at k_j^+ will be considered in the calculation of the integral.

For a positive-going wave, from Eq. (7) γ_0 either lies in the lower half-plane or may lie on the real axis for a propagating wave in an undamped waveguide. In this case there is also a pole at $-\gamma_0$ for the negative-going wave. The part of the contour along the real axis must then be indented as shown in Fig. 5. The excitation can in principle produce a pole at the origin, as shown, but this has zero residue. The residue can be calculated as [18]

$$\mathrm{Res}\left(\frac{a(z)}{b(z)}, z_0\right) = \frac{a(z_0)}{(d/dz)b(z_0)} \tag{34}$$

where $b(z_0)=0$. Hence, the residue associated with the pole at γ_0 is

$$\mathrm{Res}\left(\frac{e^{-i\gamma x_r}\overline{p}_x(\gamma)g_j^+(\gamma)}{\mu-\lambda_j^+}, \gamma_0\right) = \frac{e^{-i\gamma x_r}\overline{p}_x(\gamma)g_j^+(\gamma)}{(d/d\gamma)(\mu-\lambda_j^+)}\bigg|_{\gamma = k_j^+.} = \frac{e^{-ik_j^+ x_r}\overline{p}_x(k_j^+)g_j^+(k_j^+)}{-i\Delta e^{-ik_j^+\Delta}} = \frac{e^{-ik_j^+ x_r}\overline{p}_x(k_j^+)g_j(k_j^+)}{-i\Delta\lambda_j^+} \tag{35}$$

Thus, if x_r is to the right of the loaded area ($x_r \geq x_e$, $\forall x_e$), the contour is closed in the lower half-plane, the pole γ_0 lies within the contour of integration and

$$\begin{aligned} a_j^+(x_r) &= -2\pi i \frac{1}{\sqrt{2\pi}}\left(\frac{\overline{p}_x(k_j^+)e^{-ik_j^+ x_r}}{-i\Delta\lambda_j^+}\right)\boldsymbol{\psi}_j^+ \begin{bmatrix} \mathbf{D}_{LR}^{-1} & \mathbf{0} \\ -\mathbf{D}_{RR}\mathbf{D}_{LR}^{-1} & \mathbf{I} \end{bmatrix} \begin{Bmatrix} \mathbf{e}_L(k_j^+) \\ \mathbf{e}_R(k_j^+) \end{Bmatrix}, \\ &= \frac{2\pi\overline{p}_x(k_j^+)e^{-ik_j^+ x_r}}{\lambda_j^+\Delta\sqrt{2\pi}}\boldsymbol{\psi}_j^+ \begin{bmatrix} \mathbf{D}_{LR}^{-1} & \mathbf{0} \\ -\mathbf{D}_{RR}\mathbf{D}_{LR}^{-1} & \mathbf{I} \end{bmatrix} \begin{Bmatrix} \mathbf{e}_L(k_j^+) \\ \mathbf{e}_R(k_j^+) \end{Bmatrix} \quad j = 1,\ldots,m. \end{aligned} \tag{36}$$

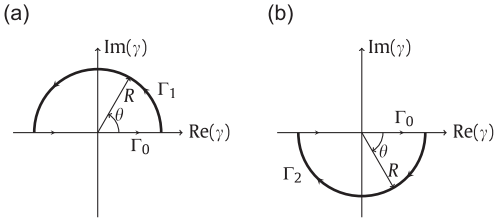

Fig. 4. Possible choices of the contour for evaluating the integral in Eq. (31).

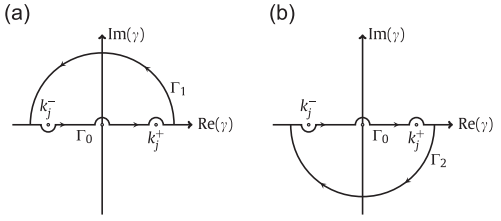

Fig. 5. Indentations of the contours: (a) $x_r \leq x_e$ and (b) $x_r \geq x_e$.

On the other hand, if x_r is to the left of the loaded area ($x_r \le x_e$, $\forall x_e$), the contour is closed in the upper half-plane and $a_j^+(x_r) = 0$.

In an analogous manner, for the negative-going wave amplitudes, if x_r is to the left of the loaded area ($x_r \le x_e$, $\forall x_e$), one finds that

$$a_j^-(x_r) = 2\pi \mathrm{i} \frac{1}{\sqrt{2\pi}} \left(\frac{\overline{p}_x(k_j^-) \mathrm{e}^{-\mathrm{i}k_j^- x_r}}{-\mathrm{i}\Delta\lambda_j^-} \right) \boldsymbol{\psi}_j^- \begin{bmatrix} \mathbf{D}_{LR}^{-1} & \mathbf{0} \\ -\mathbf{D}_{RR}\mathbf{D}_{LR}^{-1} & \mathbf{I} \end{bmatrix} \begin{Bmatrix} \mathbf{e}_L(k_j^-) \\ \mathbf{e}_R(k_j^-) \end{Bmatrix}$$
$$= -\frac{2\pi \overline{p}_x\left(k_j^-\right) \mathrm{e}^{-\mathrm{i}k_j^- x_r}}{\lambda_j^- \Delta\sqrt{2\pi}} \boldsymbol{\psi}_j^- \begin{bmatrix} \mathbf{D}_{LR}^{-1} & 0 \\ -\mathbf{D}_{RR}\mathbf{D}_{LR}^{-1} & \mathrm{I} \end{bmatrix} \begin{Bmatrix} \mathbf{e}_L(k_j^-) \\ \mathbf{e}_R(k_j^-) \end{Bmatrix}, \quad j = 1,\ldots,m, \tag{37}$$

and if x_r is to the right of the loaded area ($x_r \ge x_e$, $\forall x_e$), $a_j^-(x_r) = 0$.

The above approach still applies if $p(x, y, z) = p_x(x)p_{yz}(y, z)$ is given numerically. The Fourier transform can be used to evaluate $\overline{p}_x(k_j^{\pm})$ numerically and the external nodal forces $\mathbf{e}_L(k_j^{\pm})$ and $\mathbf{e}_R(k_j^{\pm})$ can be evaluated numerically through Eq. (21).

3.3. Response of finite waveguides

A finite waveguide excited over a span L_e is shown in Fig. 6. The wave amplitudes at various locations are also indicated. The excitation would generate positive- and negative-going waves of amplitudes $\mathbf{a}^+$ and $\mathbf{a}^-$, respectively, if it were applied to an infinite waveguide. Wave amplitudes $\mathbf{b}^+$, for example, are the superposition of the directly excited waves of amplitudes $\mathbf{a}^+$ and waves of amplitudes $\mathbf{g}^+$ after propagating across the excited region. The boundary reflection matrices relate the incident and the reflected waves as

$$\mathbf{c}^- = \mathbf{r}_R \mathbf{c}^+, \quad \mathbf{d}^+ = \mathbf{r}_L \mathbf{d}^-. \tag{38}$$

Since any boundary condition can be written as

$$\mathbf{A}\mathbf{f} + \mathbf{B}\mathbf{q} = \mathbf{0}, \tag{39}$$

and the DOFs and forces can be projected onto the wave domain, the reflection matrices can be expressed as

$$\mathbf{r}_R = -(\mathbf{A}_R\boldsymbol{\Phi}_f^- + \mathbf{B}_R\boldsymbol{\Phi}_q^-)^{-1}(\mathbf{A}_R\boldsymbol{\Phi}_f^+ + \mathbf{B}_R\boldsymbol{\Phi}_q^+) \tag{40}$$

$$\mathbf{r}_L = -(\mathbf{A}_L\boldsymbol{\Phi}_f^+ + \mathbf{B}_L\boldsymbol{\Phi}_q^+)^{-1}(\mathbf{A}_L\boldsymbol{\Phi}_f^- + \mathbf{B}_L\boldsymbol{\Phi}_q^-) \tag{41}$$

The case of a distributed load will be treated first, Fig. 6. The amplitudes of the directly excited positive- and negative-going waves generated by the distributed load acting over $L_e = x_2 - x_1$, $\mathbf{a}^+(x_2)$ and $\mathbf{a}^-(x_1)$ can be obtained via Eq. (35) and (36), respectively. Then, the amplitudes of the incident waves $\mathbf{b}$ and $\mathbf{g}$ are given by

$$\mathbf{b}^+ = [\mathbf{I} - \boldsymbol{\tau}(x_2)\mathbf{r}_L\boldsymbol{\tau}(L)\mathbf{r}_R\boldsymbol{\tau}(L-x_2)]^{-1}[\mathbf{a}^+(x_2) + \boldsymbol{\tau}(x_2)\mathrm{r}_L\boldsymbol{\tau}(x_1)\mathbf{a}^-(x_1)], \tag{42}$$

$$\mathbf{b}^- = \boldsymbol{\tau}(L-x_2)\mathbf{r}_R\boldsymbol{\tau}(L-x_2)\mathbf{b}^+, \tag{43}$$

$$\mathbf{g}^- = \mathbf{a}^- + \boldsymbol{\tau}(L_e)\mathbf{b}^-, \tag{44}$$

$$\mathbf{g}^+ = \boldsymbol{\tau}(x_1)\mathbf{r}_L\boldsymbol{\tau}(x_1)\mathbf{g}^-, \tag{45}$$

where

$$\boldsymbol{\tau}(x) = \mathrm{diag}(\mathrm{e}^{-\mathrm{i}k_1^+ x}, \ldots, \mathrm{e}^{-\mathrm{i}k_m^+ x}). \tag{46}$$

is the wave propagation matrix that gives the amplitudes of the waves after propagating a distance x. The magnitudes of all the elements of $\boldsymbol{\tau}(x)$ are ≤ 1 with the elements corresponding to high-order waves being nearly zero, thus ensuring good conditioning [15].

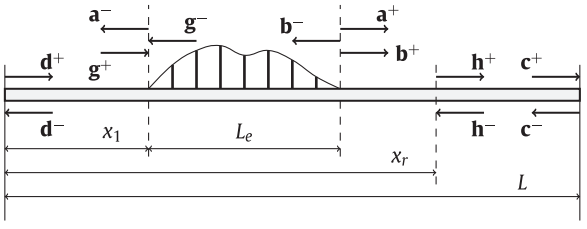

Fig. 6. Wave amplitudes in a finite waveguide excited by an arbitrary distributed load (hatched region).

The response at x_r will depend on its location with respect to the loaded span. If $x_r \geq x_2$, then

$$\mathbf{h}^+ = \boldsymbol{\tau}(x_r - x_2)\mathbf{b}^+, \tag{47}$$

$$\mathbf{h}^- = \boldsymbol{\tau}(L - x_r)\mathbf{r}_R\boldsymbol{\tau}(L - x_r)\mathbf{h}^+, \tag{48}$$

are used to obtain the response at x_r. If $x_r \leq x_1$, the wave amplitudes

$$\mathbf{h}^- = \boldsymbol{\tau}(x_1 - x_r)\mathbf{g}^-, \tag{49}$$

$$\mathbf{h}^+ = \boldsymbol{\tau}(x_r)\mathbf{r}_L\boldsymbol{\tau}(x_r)\mathbf{h}^-, \tag{50}$$

are used to evaluate the displacement at x_r. For the case where $x_1 < x_r < x_2$, the load can always be divided into two parts at x_r. Then, the amplitude of the forced waves and incident waves at x_r can be obtained for each part of the load as per Eq. (41)–(44). Finally, the superposition principle is used to find the amplitude of the incident waves at x_r. The impetus behind this is to avoid inverting $\boldsymbol{\tau}(x)$ which might be close to singular if the elements corresponding to high-order waves are nearly zero.

When a point force, f_e, is applied at x_e, the amplitude of the forced waves $\mathbf{a}^+(x_e)$ and $\mathbf{a}^-(x_e)$ can be obtained either via Eqs. (35) and (36) or via Eq. (17). Eqs. (41)–(49) still apply with x_1 and x_2 simply replaced by x_e.

4. Illustrative examples

In this section, three examples are presented to demonstrate the approach outlined above. The first is of a rod in axial vibrations excited with a point force and a constant distributed load. Analytical solutions also exist for the second example, a Euler–Bernoulli beam in bending. The third example, a three-dimensional laminated beam, is more challenging as analytical solutions are, at best, very difficult to obtain. In the following, a complex Young's modulus $\tilde{E} = E(1+i\eta)$ is used, where the loss factor η equals 3% for all the numerical cases considered.

4.1. Uniform rod in axial vibration

An infinite uniform rod undergoing axial vibration has two wavenumbers, $\pm k_a$, where [1]

$$k_a = \sqrt{\frac{\rho}{\tilde{E}}}\omega. \tag{51}$$

A concentrated axial force, f_e, acting at x=0 is considered first. The excited wave amplitudes are [1]

$$a^+ = a^- = \frac{-\mathrm{i}f_e}{2k_a\tilde{E}A}. \tag{52}$$

A segment of length Δ is taken from the rod and modeled using one element. The element has two nodes with one degree of freedom per node and a linear shape function is assumed [19]. In the WFE approach, Eq. (17) or Eqs. (41)–(49) can be used to obtain a^+ and a^- numerically. The results are normalized by the factor $\tilde{E}A/f_e\Delta$ so that

$$\hat{a}^+ = \frac{\tilde{E}A}{f_e\Delta}a^+ = \frac{-\mathrm{i}}{2k_a\Delta}. \tag{53}$$

The WFE method provides a very good estimate of the wave amplitudes at low frequency as shown in Fig. 7. As the frequency increases, the WFE results deviate from the analytical results, and the method completely breaks down near $k_a\Delta$=3.5 because of increasing FE discretization errors. For CHP excitation, there is a further issue concerning how accurately the element shape function can reproduce the nodal forces for exactly the same reasons: the element length must be small enough with respect to the wavelength of excitation.

As a second example, an axial load of intensity p_e N/m is applied to the rod between $-\xi$ and ξ. The response can be obtained analytically as

$$U(x) = \frac{p_e}{\tilde{E}Ak_a^2}\begin{cases} -\mathrm{i}\sin(\xi k_a)\mathrm{e}^{\mathrm{i}k_a x} & \text{if} \quad x \leq -\xi, \\ \cos(k_a x)\mathrm{e}^{-\mathrm{i}k_a\xi} - 1 & \text{if} \quad -\xi \leq x \leq \xi, \\ -\mathrm{i}\sin(\xi k_a)\mathrm{e}^{\mathrm{i}k_a x} & \text{if} \quad x \geq \xi. \end{cases} \tag{54}$$

Again, the results are compared in terms of the normalized displacement, defined as

$$\hat{U}(x) = \frac{\tilde{E}A}{p_e\xi^2}U(x). \tag{55}$$

To obtain the response to a distributed load, the amplitudes of the excited waves are obtained from Eqs. (35) and (36). The results are shown in Figs. 8 and 9 with Δ=ξ/20. The minima appearing in Fig. 8 occur when $k_a\xi = n\pi(n \in \mathbf{N})$. The WFE results agree very well with the theoretical results at low frequencies whether or not the response point is outside or

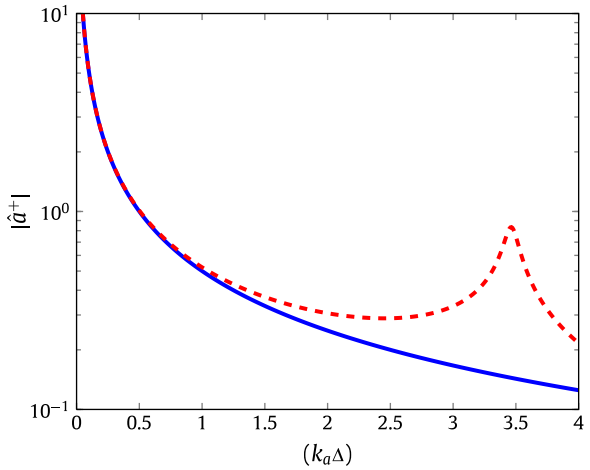

Fig. 7. Magnitude of the normalized wave amplitude $|\hat{a}^+| = |\hat{a}^-|$ of a uniform rod excited by a point force at x_e=0: — analytical results, - - WFE results.

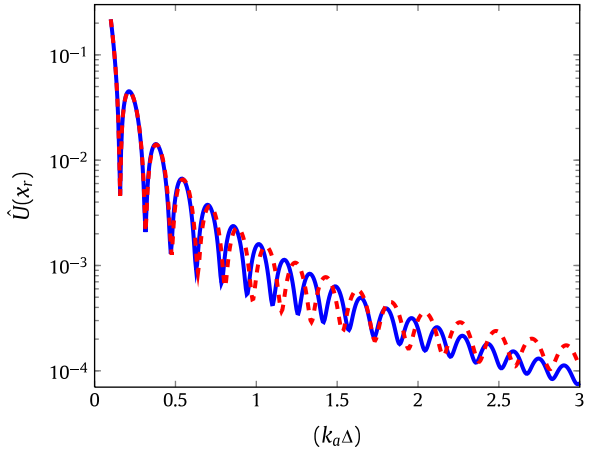

Fig. 8. Magnitude of the normalized displacement $\hat{U}$ at x_r=1.5ξ for a uniform rod excited by a uniformly distributed load: — analytical results, - - WFE results.

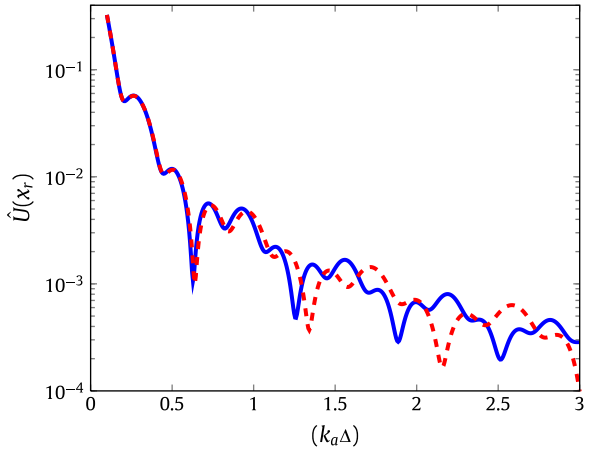

Fig. 9. Magnitude of the normalized displacement $\hat{U}$ at x_r=0.5ξ for a uniform rod excited by a uniformly distributed load: — analytical results, - - WFE results.

within the loaded span of the waveguide. Noticeable errors are apparent when $k_a\Delta > 1$. These are again attributed to FE discretization errors.

4.2. Euler–Bernoulli beam in bending

A Euler–Bernoulli beam in bending has four wavenumbers $\pm k_b$ and $\pm \mathrm{i}\, k_b$, where

$$k_b = \sqrt[4]{\frac{\rho A}{\tilde{E} I}\omega^2}. \tag{56}$$

The response to a CHP of the form $p(x) = p_e \mathrm{e}^{-\mathrm{i}\gamma x}$ is

$$W(x) = \frac{p_e}{\tilde{E} I k_b^4} \frac{1}{(\gamma/k_b)^4 - 1} \mathrm{e}^{-\mathrm{i}\gamma x}. \tag{57}$$

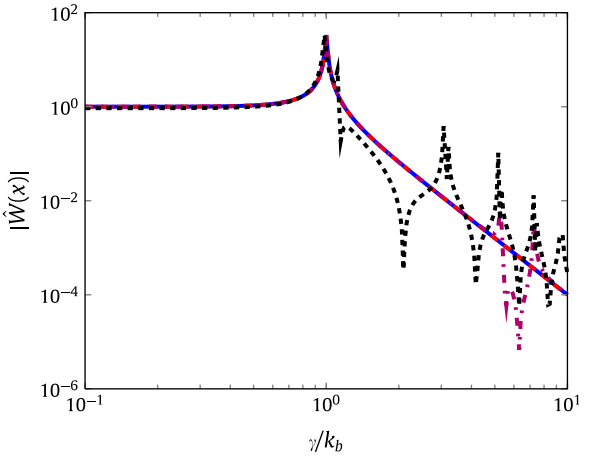

Fig. 10. Magnitude of the normalized response at x_r=0 for a Euler–Bernoulli beam excited by a CHP: — analytical, - - WFE ($k_b\Delta$=0.05), -.- WFE ($k_b\Delta$=1), ... WFE ($k_b\Delta$=3).

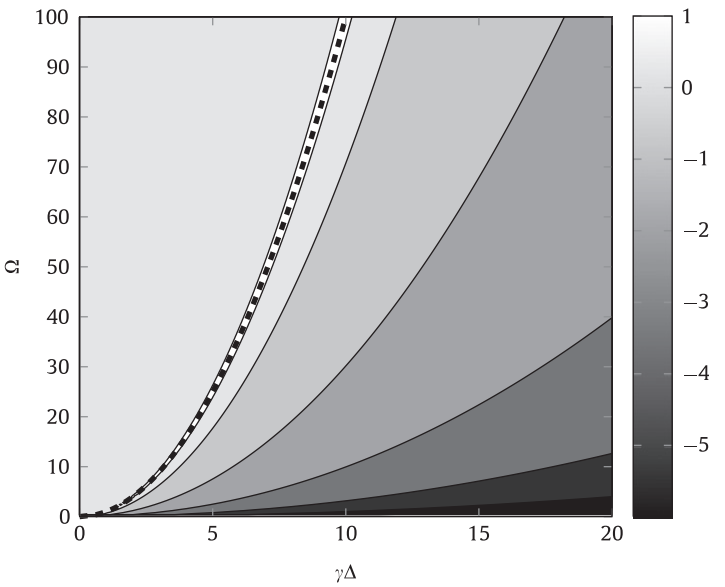

Fig. 11. Analytical response of a Euler–Bernoulli beam to a CHP: $\log_{10}|\tilde{W}(x)|$ as a function of Ω and $\gamma\Delta$. The dashed line - - represents Re($k_b\Delta$) as predicted by the WFE method.

The response can also be obtained straightforwardly via Eq. (26), and forms the kernel when obtaining the response to general loading. The analytical and WFE results will be compared in terms of a normalized response

$$\hat{W}(x) = \frac{\tilde{E}Ik_b^4}{p_e} W(x). \tag{58}$$

The normalized response is shown as a function of γ/k_b in Fig. 10. When the wavenumber ratio is small, the analytical and WFE results are in good agreement, even for relatively high frequencies ($k_b\Delta=1$), since the motion is dominated by the forcing wavenumber rather than the natural wavenumber of the beam. For very high frequencies ($k_b\Delta=3$), the WFE results deviate from the analytical solution even at low wavenumber ratio due to large FE discretization errors. At high

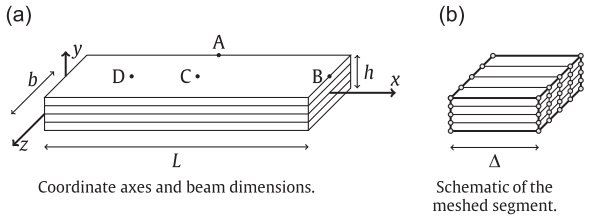

Fig. 12. Schematic of the laminated beam.

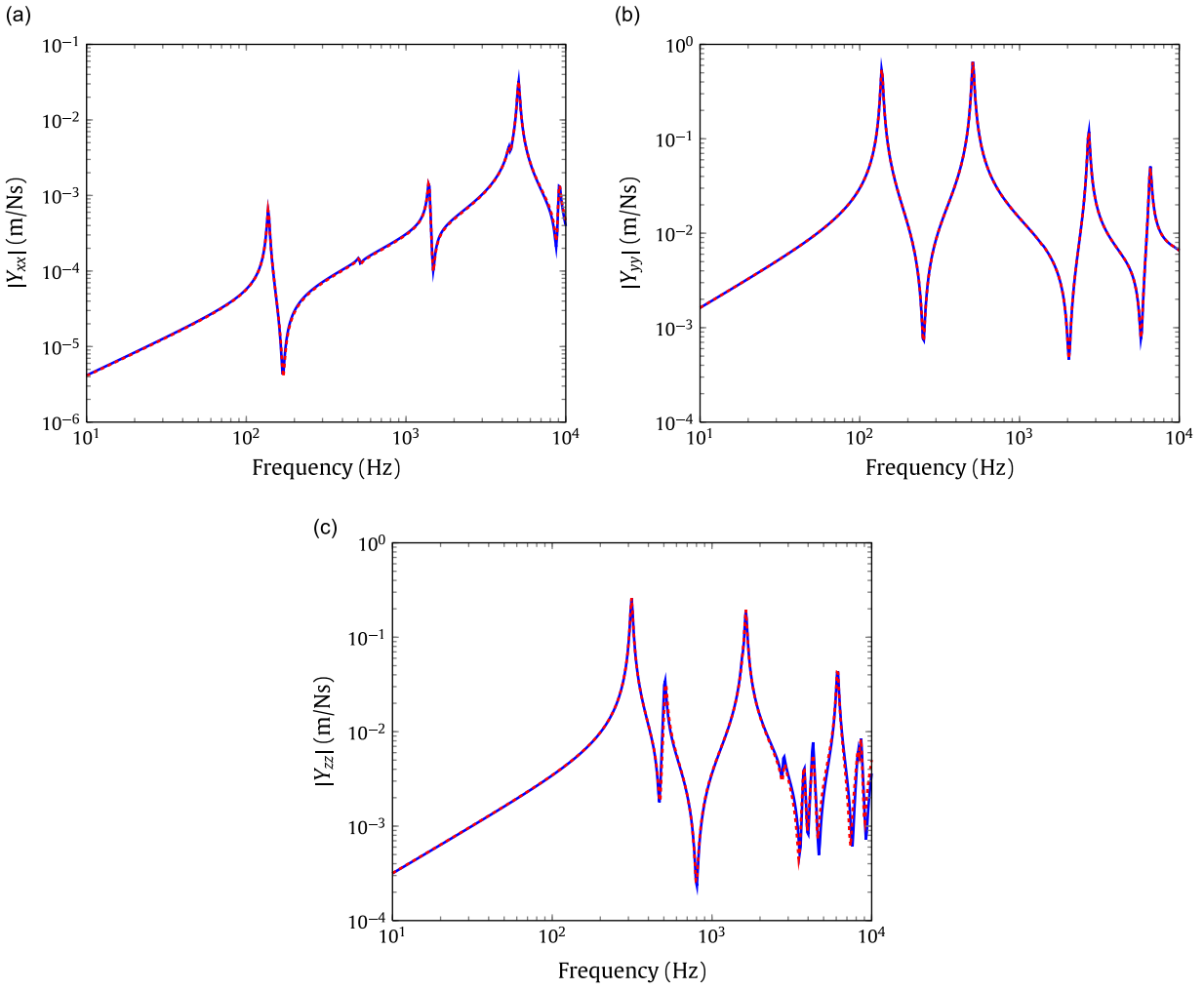

Fig. 13. Magnitude of the input mobility of the laminated beam at A in the (a) x-direction, (b) y-direction and (c) z-direction: — full FEA, - - WFE results with 11 wavemodes retained.

wavenumber ratios, the WFE results deviate from the analytical results as the forcing wavelength becomes small compared to the segment's length. FE discretization errors arise in the calculation of the nodal forces if the element length is too large compared to the wavelength of the excitation.

The response of a Euler–Bernoulli beam to a CHP can be further illustrated by introducing the dimensionless quantities

$$\tilde{W}(x) = \frac{\tilde{E}I}{p_e \Delta^4} W(x), \quad \boldsymbol{\Omega} = \sqrt{\frac{\rho A}{\tilde{E}I}} \Delta^2 \omega. \tag{59}$$

Fig. 11 shows the response to a CHP as a function of the dimensionless frequency and wavenumber. The response is small except when the forcing wavenumber is near the free wavenumber of the beam. Furthermore, the free wavenumber of the beam can be traced at the projection of the maximum values of the response as shown in Fig. 11.

4.3. Cantilevered laminated beam

The third example is of a cantilevered beam, comprising four orthotropic layers of 1mm thick glass-epoxy, Fig. 12. The stacking sequence is $[0/45/-45/0]$ degrees, and the material properties of each glass-epoxy layer along the axes x', y' and z' of orthotropy are $E_{x'} = E_{z'} = 54 \times 10^9$, $E_{y'} = 4.8 \times 10^9$, $G_{x'y'} = G_{z'y'} = 1.78 \times 10^9$, $G_{x'z'} = 3.16 \times 10^9$, $\nu_{x'y'} = \nu_{z'y'} = 0.313$, $\nu_{x'z'} = 0.06$, and $\rho = 2000$. The dimensions of the beam are $L = 0.2$, $b = 0.02$ and $h = 0.004$. ANSYS® was used to model the structure with SOLID45 elements of length $\Delta = 2$ mm. Each layer was discretized using four elements and hence the segment has 16, eight-noded elements with three translational DOFs per node. Thus, there are 75 DOFs on each side of

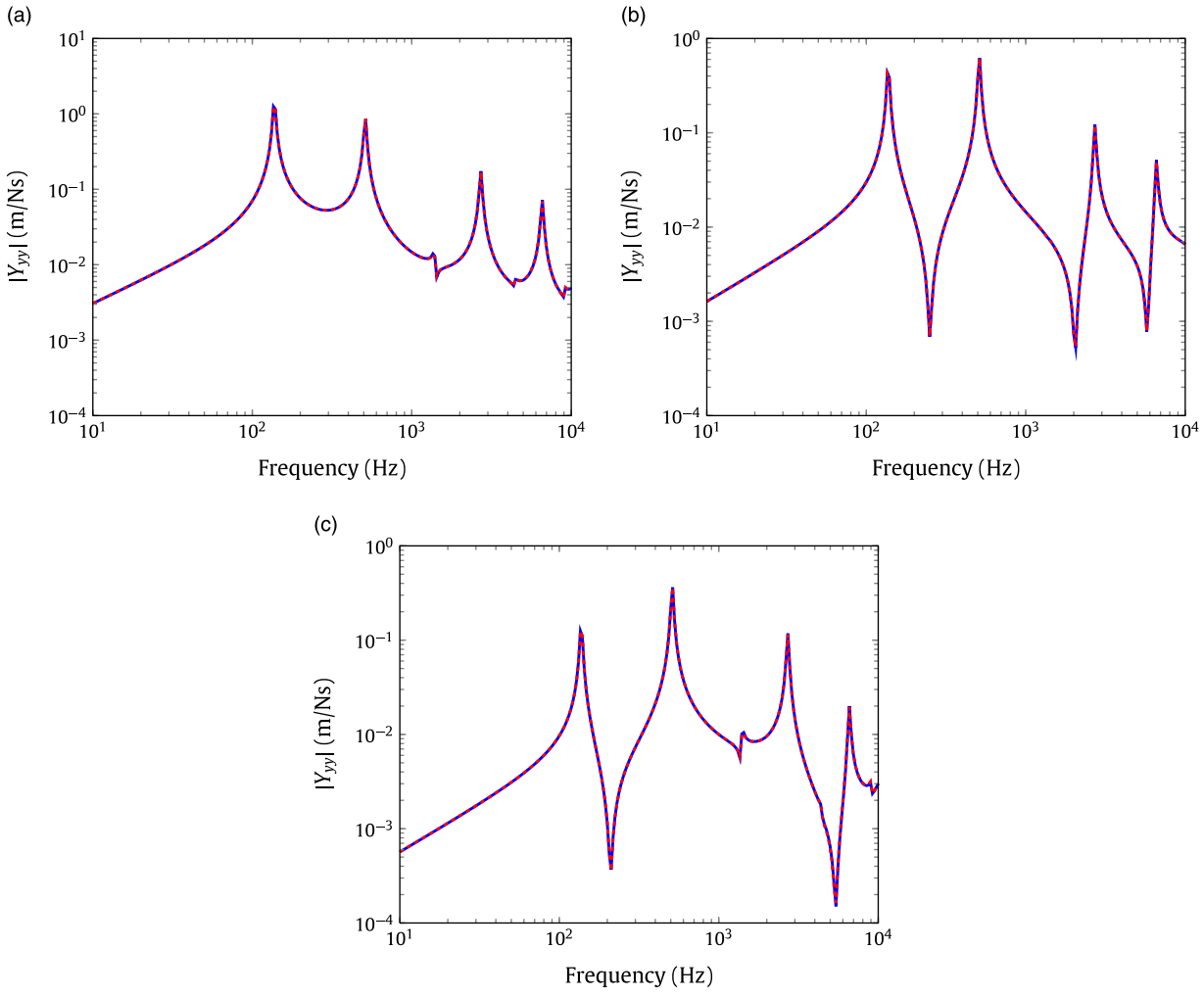

Fig. 14. Magnitude of the transfer mobility of the laminated beam in the y-direction at (a) B, (b) C and (c) D: — full FEA, - - WFE results with 11 wavemodes retained.

the segment. Using the coordinate system of Fig. 12, the following points are defined: $A(0.5L, h/2, -b/2)$, $B(L, h/2, 0)$, $C(L/2, h/2, 0)$ and $D(L/4, h/2, 0)$.

When the eigenvalue problem of Eq. (4) is solved, 75 pairs of (positive- and negative-going) waves are obtained. Wavemodes with sufficiently small $|\mathrm{Im}(k\Delta)|$ are retained to calculate the forced response. Most of the wavemodes obtained are strongly decaying waves at each frequency, and their contribution to the response is thus negligible. Moreover, the prediction of the wavemodes is likely to be inaccurate due to the presence of eigenvalues of very small and very large magnitudes [15]. As mentioned in Section 2.1, the eigenvalue problem can be recast into a better-conditioned form to avoid numerical problems.

In the numerical example, at each frequency only those wavemodes for which $|\mathrm{Im}(k\Delta)| < 0.3$ are retained for the WFE predictions. There are up to 11 pairs of (positive- and negative-going) waves at each frequency in the frequency range considered, where four pairs are propagating waves and the remaining are evanescent waves. The WFE predictions are compared with those of the full FE model of the beam (meshed with the same element size). The full FE model contains 7575 DOFs whereas the WFE model has only 75 DOFs.

First, the input mobilities in the x-, y- and z-directions at A are evaluated. The WFE and full FEA results are in very good agreement as shown in Fig. 13. The beam's highest stiffness is in the x-direction and it is most flexible in the y-direction. The first mode of motion in the x- and y-directions occurs at the same frequency due to geometric and material coupling between the two directions. Although the response of the second mode in the x-direction is small, a substantial response is observed in the y- and z-directions at the same frequency because of the anisotropy of the beam. The WFE and full FEA predictions are indistinguishable, except for the off-resonance response for the mobility in the z-direction at high frequencies.

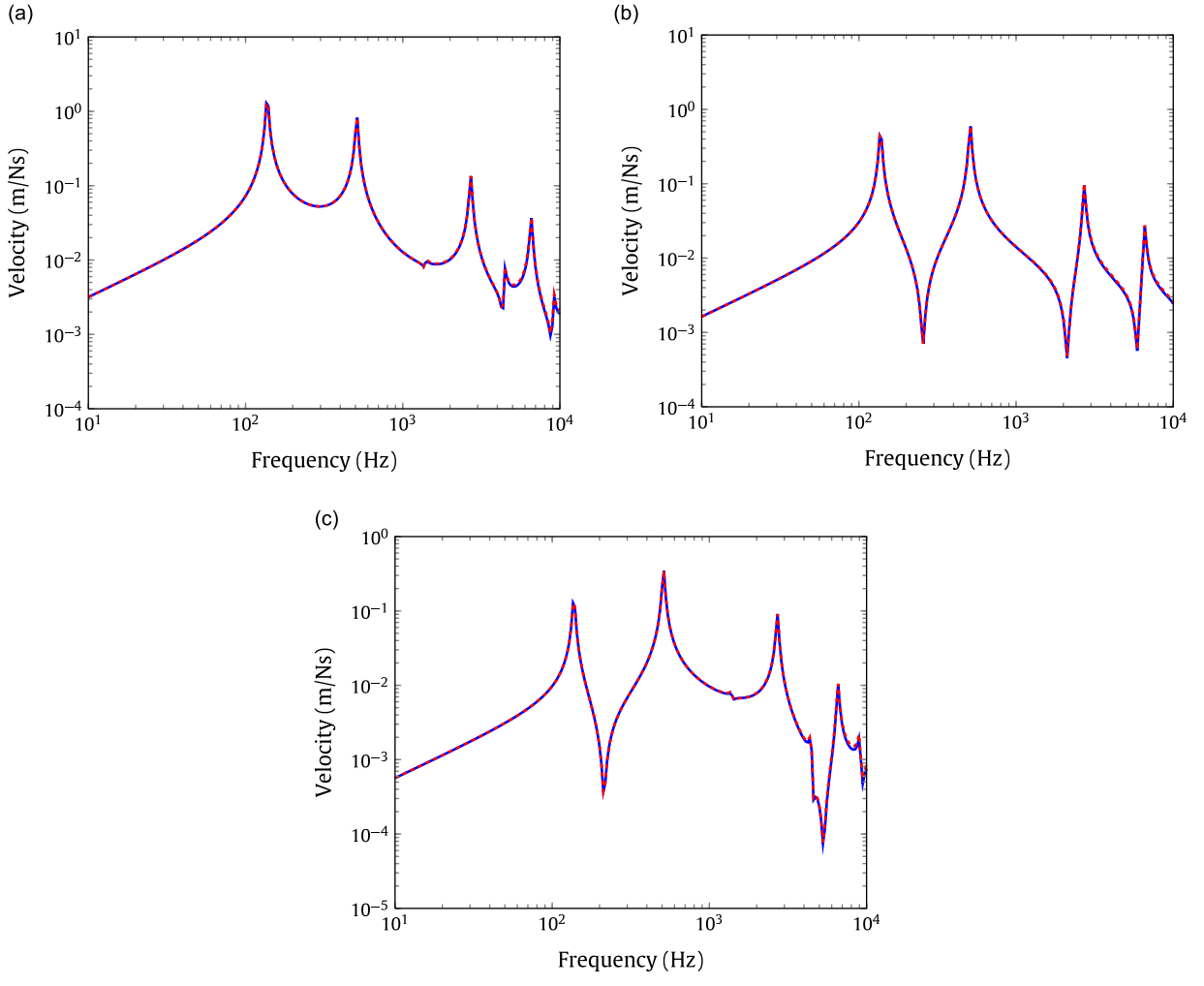

Fig. 15. Response of the laminated beam in the y-direction to distributed loading at (a) B, (b) C and (c) D: — full FEA, - - WFE results with 11 wavemodes retained.

Next, a unit force in the y-direction is applied at A and the transfer mobility in the y-direction is evaluated at B, C and D. The transfer mobilities at the response points evaluated using the WFE method with 11 wavemodes are in very good agreement with the full FEA solution as shown in Fig. 14.

Now consider the response to a uniformly distributed load with unit intensity. The loading is in the y-direction, acting on the top surface between $x_1=0.4L$ and $x_2=0.6L$ and across the full width of the beam. The velocity in the y-direction is evaluated using the WFE method and contour integration approach with only 11 pairs of (positive- and negative-going) waves. The response was evaluated at B, C and D. At low frequencies, the response to the distributed load is almost the same as that of the point force shown in Fig. 14. Whether or not the response point is within or outside the loaded area, the WFE results are in very good agreement with the results obtained via the full FEA as shown in Fig. 15. For the response at C, disagreement between the WFE and full FEA responses are observed off-resonance at high frequencies. Moreover, at higher frequencies, the response tends to be smaller than that of a point force due to the distributed nature of the loading.

5. Conclusions

This paper concerns the forced response of waveguides using the wave and finite element method. The formulation is based on obtaining the response of the waveguide to a convected harmonic pressure, and using that as a kernel for the response to a general loading which is found by Fourier transform and contour integration. The integral is evaluated analytically so that the computation time is very small. This yields the amplitudes of the excited waves, and from them and the system propagation and reflection properties the frequency response functions of waveguides follow.

Waveguides with arbitrarily complex cross-sections can be considered, and the numerical results are accurate if the FE mesh is small enough. A reduced wave basis can be used and the methods described in Ref. [15] can be used to circumvent numerical problems.

Acknowledgements

The authors gratefully acknowledge the financial support provided by the Engineering and Physical Sciences Research Council under grant number EP/F069391/1 and the European Commission in the context of the collaborative project "Mid-Mod: Mid-frequency vibro-acoustic modelling tools - innovative CAE methodologies to strengthen European competitiveness" (Grant agreement number: 218508).

References

[1] K.F. Graff, in: *Wave Motion in Elastic Solids*, Dover Publications Inc., New York, 1975.
[2] C.-M. Nilsson, *Waveguide Finite Elements Applied on a Car Tyre*, KTH, Stockholm, 2004.
[3] F. Birgersson, *Prediction of Random Vibration using Spectral Methods*, KTH, Stockholm, 2004.
[4] S. Finnveden, Evaluation of modal density and group velocity by a finite element method, *Journal of Sound and Vibration* 273 (2004) 51–75.
[5] B.R. Mace, D. Duhamel, M.J. Brennan, L. Hinke, Finite element prediction of wave motion in structural waveguides, *Journal of the Acoustical Society of America* 117 (5) (2005) 2835–2843.
[6] D. Duhamel, B.R. Mace, M.J. Brennan, Finite element analysis of the vibrations of waveguides and periodic structures, *Journal of Sound and Vibration* 294 (1–2) (2006) 205–220.
[7] L. Gry, C. Gontier, Dynamic modelling of railway track: a periodic model based on a generalized beam formulation, *Journal of Sound and Vibration* 199 (4) (1997) 531–558.
[8] D.J. Thompson, Wheel–rail noise generation, part I: introduction and interaction model, *Journal of Sound and Vibration* 161 (3) (1993) 387–400.
[9] L. Houillon, M.N. Ichchou, L. Jezequel, Wave motion in thin-walled structures, *Journal of Sound and Vibration* 281 (3-5) (2005) 483–507.
[10] M. Maess, N. Wagner, L. Gaul, Dispersion curves of fluid filled elastic pipes by standard FE models and eigenpath analysis, *Journal of Sound and Vibration* 296 (1–2) (2006) 264–276.
[11] J.-M. Mencik, M.N. Ichchou, Wave finite elements in guided elastodynamics with internal fluid, *International Journal of Solids and Structures* 44 (7–8) (2007) 2148–2167.
[12] B.R. Mace, E. Manconi, Modelling wave propagation in two-dimensional structures using finite element analysis, *Journal of Sound and Vibration* 318 (4–5) (2008) 884–902.
[13] E. Manconi, B.R. Mace, Wave characterization of cylindrical and curved panels using a finite element method, *Journal of the Acoustical Society of America* 125 (1) (2009) 154–163.
[14] Y. Waki, B.R. Mace, M.R. Brennan, Free and forced vibrations of a tyre using a wave/finite element approach, *Journal of Sound and Vibration* 323 (3–5) (2009) 737–756.
[15] Y. Waki, B.R. Mace, M.J. Brennan, Numerical issues concerning the wave and finite element method for free and forced vibrations of waveguides, *Journal of Sound and Vibration* 327 (1–2) (2009) 92–108.
[16] W.X. Zhong, F.W. Williams, On the direct solution of wave propagation for repetitive structures, *Journal of Sound and Vibration* 181 (3) (1995) p. 485–485.
[17] W.X. Zhong, F.W. Williams, A.Y.T. Leung, Symplectic analysis for periodical electro-magnetic waveguides, *Journal of Sound and Vibration* 267 (2) (2003) 227–244.
[18] J.E. Marsden, M.J. Hoffman, *Basic Complex Analysis*, W.H. Freeman & Co. Ltd., 1999.
[19] M. Petyt, *Introduction to Finite Element Vibration Analysis*, Cambridge University Press, New York, 1990.